

pubs.acs.org/acsaelm Article

# Spatially Resolved Investigation of the Bandgap Variation across a $\beta$ -(Al<sub>x</sub>Ga<sub>1-x</sub>)<sub>2</sub>O<sub>3</sub>/ $\beta$ -Ga<sub>2</sub>O<sub>3</sub> Interface by STEM-VEELS

Adrian Chmielewski, Ziling Deng, Parivash Moradifar, Leixin Miao, Yuewei Zhang, Akhil Mauze, Kleyser A. Lopez, Wolfgang Windl, and Nasim Alem\*



Cite This: ACS Appl. Electron. Mater. 2022, 4, 585-591



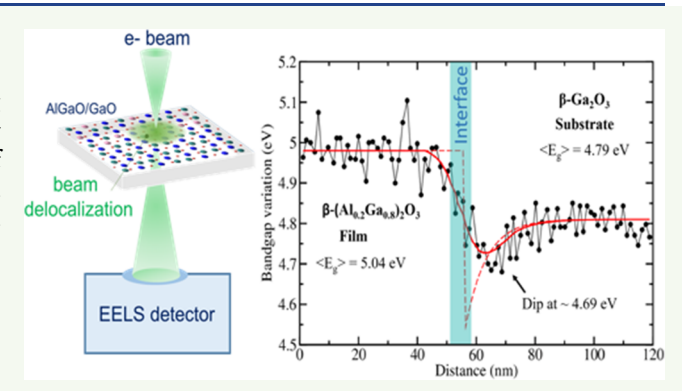
**ACCESS** I

Metrics & More

Article Recommendations

s Supporting Information

**ABSTRACT:** Alloying β-(Al<sub>x</sub>Ga<sub>1-x</sub>)<sub>2</sub>O<sub>3</sub> on a β-Ga<sub>2</sub>O<sub>3</sub> substrate results in a heterojunction with a tunable bandgap, but is often plagued by defects in the interface region. In this work, using valence electron energy loss spectroscopy combined with density functional theory calculations, we identify a high concentration of cation interstitials at a β-(Al<sub>0.2</sub>Ga<sub>0.8</sub>)<sub>2</sub>O<sub>3</sub>/β-Ga<sub>2</sub>O<sub>3</sub> interface and measure the optical absorption edge. We find a dip in the band edge of 0.1 eV depth and a width of around 15 nm on the β-Ga<sub>2</sub>O<sub>3</sub> side of the interface with signs of noticeable electron probe delocalization broadening and discuss defect states versus excitons as its possible origins.



KEYWORDS: ultra-wide-bandgap, beta-gallium-oxide, TEM, EELS, point defects, interstitials

# INTRODUCTION

Beta gallium oxide ( $\beta$ -Ga<sub>2</sub>O<sub>3</sub>) is a semiconductor that has caught considerable attention in the field of electronics due to its wide bandgap (4.6–4.9 eV) and a predicted high breakdown field (8 MV/cm) that is much larger than SiC and GaN.<sup>1</sup> These high potentials will set up new standards in a wide range of next-generation electronic and optoelectronic applications.<sup>1,2</sup> The limits can be pushed even further by alloying  $\beta$ -Ga<sub>2</sub>O<sub>3</sub> with aluminum (Al) that would allow bandgap engineering of ultrawide bandgap alloys.

As the stable corundum phase of  $Al_2O_3$  has a bandgap of 8.82 eV and its monoclinic phase has a predicted bandgap of 7.24 eV,  $(Al_xGa_{1-x})_2O_3$  alloys would permit to explore a larger field of possibilities in power electronic devices, enabling larger bandgaps with more tunability and higher breakdown voltages. These alloys could also cover a deeper spectrum in the ultraviolet (UV) region and drastically enhance the performance of detectors. For instance, it has been recently shown that the performance of deep-UV  $\beta$ - $(Al_xGa_{1-x})_2O_3$ -based photovoltaic detectors are increased by 1–2 orders of magnitude as compared to unalloyed  $Ga_2O_3$ .

The bandgap of  $\beta$ - $(Al_xGa_{1-x})_2O_3$  has been recently studied over the whole range of the alloy composition using various techniques.  $^{5-14}$ 

Zhang et al. reported bandgaps in the 5.2–7.1 eV range for Al content between 0.24 and 1 in  $\beta$ -(Al<sub>x</sub>Ga<sub>1-x</sub>)<sub>2</sub>O<sub>3</sub> thin films using X-ray photoelectron spectroscopy (XPS). Similarly, using XPS, Krueger et al. reported the bandgap of  $\beta$ -(Al<sub>x</sub>Ga<sub>1-x</sub>)<sub>2</sub>O<sub>3</sub> to increase linearly with local stoichiometry

within the 4.8–6.6 eV range for the composition x going from 0 to  $1.^{16}$  Density functional theory (DFT) with the Heyd–Scuseria–Ernzerhof hybrid functional calculations have also shown a bandgap in the range of 4.69–7.03 eV for  $\beta$ -(Al<sub>x</sub>Ga<sub>1-x</sub>)<sub>2</sub>O<sub>3</sub>. These studies, however, lack the spatial resolution and cannot consider the effect of defects on the electronic structure that are frequently found near the interface, although defects are known to create defect states in the bandgap. Considering that, the understanding of the effect of these defects is important because it can directly link the atomic structure to the electronic properties in the device.

To quantitatively study the band structure and optical properties of the  $\beta$ - $(Al_xGa_{1-x})_2O_3/\beta$ - $Ga_2O_3$  system in the nanoscale regime, we use high-resolution scanning transmission electron microscopy (STEM) imaging coupled with valence electron energy loss spectroscopy (VEELS). <sup>17,18</sup> Similar to optical microscopy, the low-loss region of an EELS spectrum (0–50 eV) provides a wide range of information about the band structure and particularly about the dielectric function of the material. <sup>19–21</sup> In addition to the collective excitation modes that give rise to surface and bulk

Received: September 7, 2021 Accepted: January 9, 2022 Published: January 24, 2022





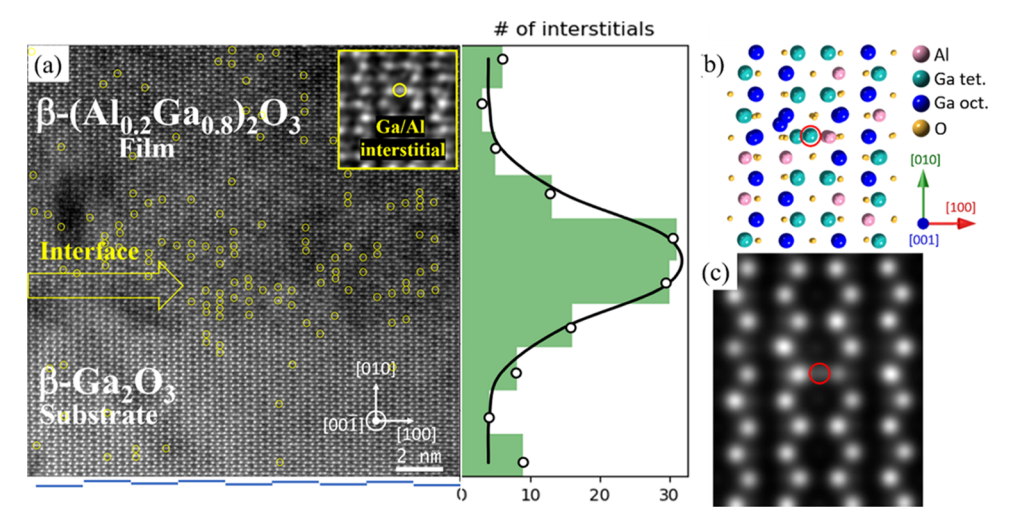


Figure 1. (a) HAADF–STEM image of the β-(Al<sub>0.2</sub>Ga<sub>0.8</sub>)<sub>2</sub>O<sub>3</sub>/β-Ga<sub>2</sub>O<sub>3</sub> interface. All the Ga/Al interstitials are highlighted by yellow circles. Inset: zoomed-in image of a single Ga or Al interstitial that forms the di-interstitial vacancy complex. Yellow arrow: β-(Al<sub>0.2</sub>Ga<sub>0.8</sub>)<sub>2</sub>O<sub>3</sub>/β-Ga<sub>2</sub>O<sub>3</sub> interface. The histogram with the interstitial distribution (green bars) can be well fitted with a Gaussian of width 2.1 nm (black line). (b) DFT relaxed crystal structure of β-(Al<sub>0.2</sub>Ga<sub>0.8</sub>)<sub>2</sub>O<sub>3</sub> in [001] projection with one Ga interstitial highlighted by the red circle and (c) its corresponding HAADF–STEM simulated image showing the atomic contrast of the Ga interstitial. The case for Al interstitial is shown in Figure S2 of Supporting Information.

plasmon peaks, interband and intraband transitions can also be efficiently measured through the excitation of single valence electrons from the ground state to unoccupied states of higher energy.<sup>22</sup> The energy region of the bandgap can be investigated if it is usually larger than the width of the zero-loss peak (ZLP), which is true for  $\beta$ -(Al<sub>x</sub>Ga<sub>1-x</sub>)<sub>2</sub>O<sub>3</sub> alloys. The viability of EELS for bandgap measurements has in the past been hindered by the limited energy resolution of conventional TEMs (down to about 0.3 eV for microscopes equipped with cold field emission electron sources). <sup>23,24</sup> However, the development of monochromator systems and high-resolution EELS detectors over the past decades allows now to achieve an energy resolution of better than 0.1 eV for the most advanced instruments. 25,26 Moreover, as the electronic properties of a material are often directly affected by its crystal structure and the presence of defects such as vacancies and interstitials, it is crucial to be able to extract precise electronic structure information at high spatial resolution. The VEELS technique is therefore an excellent way to accomplish these challenging tasks as it can probe the electronic properties of a given material in the nanoscale regime with high energy resolution. Many results on bandgap measurements using STEM-VEELS have been reported over the past few years including nanoscale mapping of bandgap gradients in thin films, <sup>27–29</sup> bandgaps in two-dimensional (2D) films,<sup>30</sup> band line-ups at interfaces,<sup>31</sup> dielectric functions,<sup>31–34</sup> and thickness-dependent bandgap measurements.<sup>35</sup> However, the spatially resolved bandgap variation in  $\beta$ -(Al<sub>x</sub>Ga<sub>1-x</sub>)<sub>2</sub>O<sub>3</sub> thin films and its link to their crystal structure are yet to be understood.

In the current work, a  $\beta$ -(Al<sub>x</sub>Ga<sub>1-x</sub>)<sub>2</sub>O<sub>3</sub> thin film grown by molecular beam epitaxy on a  $\beta$ -Ga<sub>2</sub>O<sub>3</sub> substrate has been investigated by STEM-VEELS. Here, we show the atomic structure of the crystal and the nanoscale variations in the adsorption edge across the  $\beta$ -(Al<sub>x</sub>Ga<sub>1-x</sub>)<sub>2</sub>O<sub>3</sub>/ $\beta$ -Ga<sub>2</sub>O<sub>3</sub> interface using high-resolution STEM-EELS. We perform a quantitative analysis of the concentration of cation interstitials at the interface which can be directly observed and find that they are concentrated over a narrow distribution with a width of 2 nm at the interface. We also find a dip in the absorption edge of 0.1 eV depth and a width between 15 and 20 nm on the  $\beta$ -Ga<sub>2</sub>O<sub>3</sub>

side of the interface and investigate its origin by regression analysis of the measured spectrum in combination with DFT and Poisson solver-based band modeling.

#### RESULTS AND DISCUSSION

Defects can have a profound effect on the electronic properties of crystals. Currently, a significant effort is focused on the growth of clean, defect-free  $(Al_xGa_{1-x})_2O_3$  thin films via different growth techniques such as metal-organic chemical vapor deposition, 36-39 pulsed laser deposition, 15,40 lowpressure reactive vapor deposition,<sup>5</sup> and molecular beam epitaxy. 41 Although small defect-free regions in monoclinic films of  $\beta$ -(Al<sub>0.4</sub>Ga<sub>0.6</sub>)<sub>2</sub>O<sub>3</sub> with 10 nm thickness and  $\beta$ - $(Al_{0.26}Ga_{0.74})_2O_3$  with 30–40 nm thickness have been observed, the growth of defect-free  $\beta$ - $(Al_xGa_{1-x})_2O_3$  thin films remains challenging. In this work, we uncover the defect structure in a  $\beta$ -(Al<sub>x</sub>Ga<sub>1-x</sub>)<sub>2</sub>O<sub>3</sub> thin film using aberrationcorrected scanning transmission electron microscope equipped with an EELS detector. Figure 1a shows a high-angle annular dark-field (HAADF)—STEM image of the  $\beta$ -(Al<sub>0.2</sub>Ga<sub>0.8</sub>)<sub>2</sub>O<sub>3</sub>/ $\beta$ -Ga<sub>2</sub>O<sub>3</sub> interface, in the [001] projection, imaged at 300 kV. A first analysis by energy-dispersive X-ray spectroscopy shows an Al content of  $x = (20 \pm 2)$  % in this sample (Figure S1 of Supporting Information). As the contrast in dark-field imaging increases with the Z number of the element, the overall contrast of the film is lower than that of the substrate due to the presence of Al atoms with a lower atomic number (Z = 13)than Ga (Z = 31). The rough interface is indicated by the yellow arrow. Moreover, a closer look at the  $\beta$ -(Al<sub>0.2</sub>Ga<sub>0.8</sub>)<sub>2</sub>O<sub>3</sub> film uncovers different defects in the crystal structure. A zoomed-in image of an area in the film that shows a Ga/Al interstitial sitting in between two tetrahedral Ga/Al atoms is shown in the inset and highlighted by the yellow circle. The population of the Al/Ga interstitials across the interface is plotted on the right of Figure 1a. According to this plot, the number of interstitials is maximal at the  $\beta$ -(Al<sub>0.2</sub>Ga<sub>0.8</sub>)<sub>2</sub>O<sub>3</sub>/ $\beta$ -Ga<sub>2</sub>O<sub>3</sub> interface and can be fitted with a Gaussian distribution of width 2.1 nm as shown. The absolute concentration cannot be determined from this 2D image. To explore the nature of these interstitials, DFT calculations have been performed and

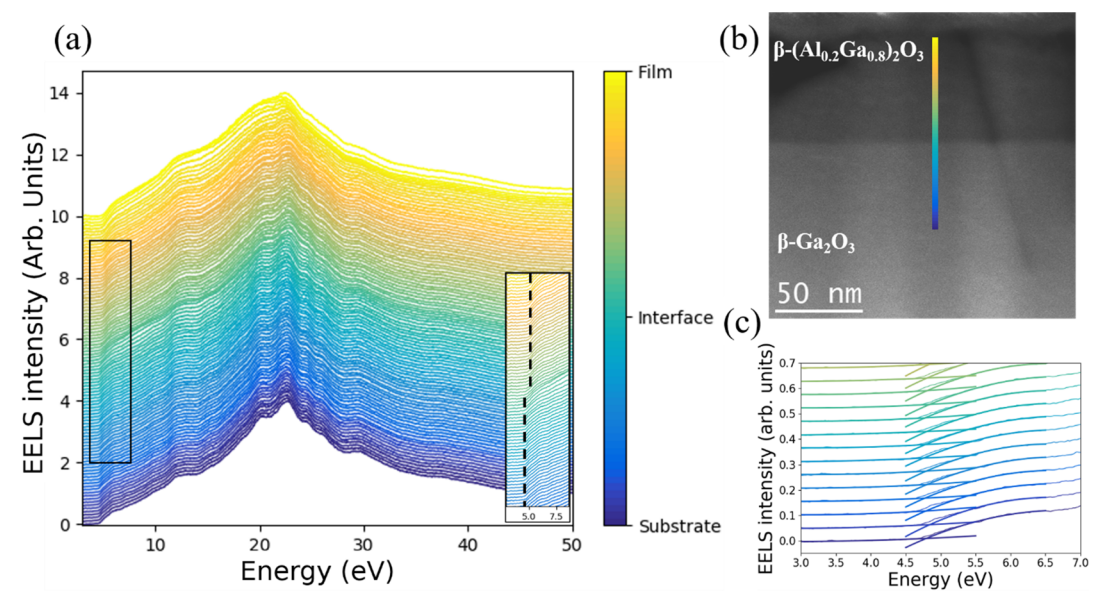


Figure 2. (a) Low-loss EELS spectra extracted from the EELS line scan across the β- $(Al_{0.2}Ga_{0.8})_2O_3/β$ - $Ga_2O_3$  interface. Inset: zoom-in on the blue shift of the bandgap indicated by the dashed lines. (b) Low magnification HAADF–STEM image showing the localization of the line scan across the interface. (c) Polynomial fitting method used for bandgap extraction. The bandgap is determined from the intersection of the two polynomial functions.

have shown that both Al and Ga atoms can be stabilized in the interstitial site. Furthermore, the Al/Ga interstitial tends to push its nearest neighbor out of its initial position creating a diinterstitial-vacancy complex. Figure 1b shows the relaxed crystal structure of  $\beta$ -(Al<sub>0.2</sub>Ga<sub>0.8</sub>)<sub>2</sub>O<sub>3</sub> in [001] projection with a single Ga interstitial highlighted by a red circle sitting in between tetrahedrally coordinated Ga and Al atoms. To uncover the contrast of the Ga interstitial, a HAADF-STEM image was simulated using the relaxed crystal structure shown in Figure 1b (simulation details in the Supporting Information). According to the simulated image shown in Figure 1c, the interstitial Ga atoms are observed to have a dim contrast in agreement with what is observed experimentally. Al interstitials at this position and with our experimental image conditions are invisible as observed in the experiment and confirmed with image simulations (Figure S2 of Supporting Information). Thus, all detected interstitials in Figure 1a should be Ga interstitials.

The high defect density especially in the vicinity of the interface makes it crucial to understand how these defect complexes affect the electronic structure of the material in the  $\beta$ -(Al<sub>0.2</sub>Ga<sub>0.8</sub>)<sub>2</sub>O<sub>3</sub> film. We have performed low-loss EELS combined with STEM to determine the bandgap of the film across the interface (the experimental details can be found in the Supporting Information). The deconvoluted low-loss EELS spectra across the interface with a cutoff energy of 50 eV are shown in Figure 2a. The colored bar indicates the different regions of the sample and the localization of the line scan across the interface is shown in Figure 2b. The intense peak around 22.3 eV is the volume plasmon peak of  $\beta$ - $(Al_rGa_{1-r})_2O_3$ . The inset on the bottom right shows a rough estimate of the bandgap indicated by the black dashed lines. To precisely extract the bandgap variation across the  $\beta$ - $(Al_{0.2}Ga_{0.8})_2O_3/\beta$ -Ga<sub>2</sub>O<sub>3</sub> interface, we have used two polynomial functions to fit the flat region before the plasmon and the start of the plasmon peak as shown in Figure 2c. The bandgap was then extracted by taking the intersection of the

two fitting curves, as previously proposed in the literature.  $^{29,30,32,43}$ 

The resulting variation of the bandgap as a function of the line scan distance is shown in Figure 3. The mean value of the

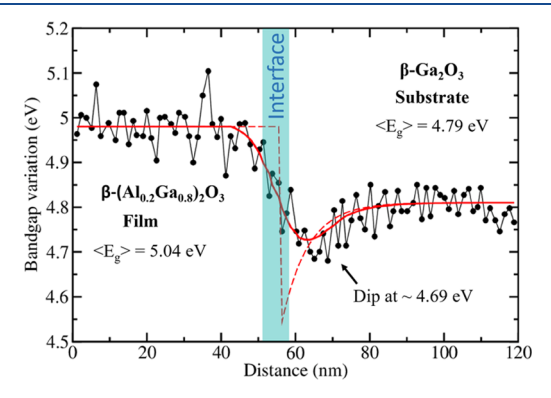


Figure 3. Experimental VEELS bandgap values (black dots) vs theoretical bandgap from assuming defect states at the interface that lower the bandgap to 4.57 eV as measured in ref 44, exponentially decaying into  $\beta$ -Ga<sub>2</sub>O<sub>3</sub> with a decay length of 7 nm (red dashed line), convoluted with 15 nm Lorentzian broadening (red solid line).

measured bandgap is  $E_{\rm g}=4.79\pm0.1$  eV for  $\beta\text{-}{\rm Ga_2O_3}$  (x=0) and  $E_{\rm g}=5.04\pm0.1$  eV for  $\beta\text{-}{\rm (Al_{0.2}Ga_{0.8})_2O_3}$ , both in excellent agreement with reported values in the literature.

The bandgap change of 0.25 eV observed across the  $\beta$ - $(Al_{0.2}Ga_{0.8})_2O_3/\beta$ - $Ga_2O_3$  interface is smaller than a recent theoretical value of 0.47 eV for the  $\beta$ - $(Al_{0.2}Ga_{0.8})_2O_3/\beta$ - $Ga_2O_3$  interface, <sup>10</sup> but is in excellent agreement with our DFT result of 0.22 eV as shown in Figure S7c. In addition, a  $\sim$ 0.1 eV dip in the bandgap is observed within the substrate, right below the  $\beta$ - $(Al_{0.2}Ga_{0.8})_2O_3/\beta$ - $Ga_2O_3$  interface, as indicated by the arrow in Figure 3, before it reaches the constant energy value of 4.79 eV. The width of the interface has been determined to be 6 nm using the contrast variation in the HAADF–STEM image extracted from the intensity profile and determined by

regression as described in the Supporting Information (Figure S5 of Supporting Information along with eqs S1–S4). However, this value should be considered as an upper limit because the conditions of the image acquisition, such as the gain and the defocus, can induce errors in the interface width determination.

The observed dip in the bandgap could be caused by several different factors which we examine in the following, which are strain, bandgap renormalization, excitons, and deep electron states from the interface interstitials or from other defects. First, it is known that alloying  $\beta$ -Ga<sub>2</sub>O<sub>3</sub> with Al<sub>2</sub>O<sub>3</sub> can slightly affect the lattice parameters of the crystal, especially along the b axis [010]<sup>16</sup> and thus have an impact on the electronic properties. Figure S3 in Supporting Information shows DFT calculated lattice parameters for a, b, and c axes for  $\beta$ -Ga<sub>2</sub>O<sub>3</sub>,  $Al_2O_3$ , and  $\beta$ - $(Al_{0.2}Ga_{0.8})_2O_3$ . It is shown that the lattice parameter in the b direction decreases about 1.1% upon alloying. However, this small variation in the lattice parameter does not induce any significant localized strain especially in the substrate where the dip is observed, which is also confirmed by geometric phase analysis as shown in Figure S4 of Supporting Information. Thus, strain cannot explain the observed dip in the bandgap across the  $\beta$ -(Al<sub>0.2</sub>Ga<sub>0.8</sub>)<sub>2</sub>O<sub>3</sub>/ $\beta$ -Ga<sub>2</sub>O<sub>3</sub> interface.

Another hypothesis for the bandgap shrinkage near the interface can be related to the renormalization effect, 45 where in heavily *n*-doped semiconductors, the interactions between free carriers and ionized impurities will induce a downward shift of the conduction band (and an upward shift of the valence band), eventually decreasing the fundamental bandgap energy. Our DFT calculations show that in order to decrease the bandgap by 0.1 eV, electron concentrations in excess of 10<sup>21</sup> cm<sup>-3</sup> would be necessary (Figure S8). For these concentrations, the Fermi level moves into the conduction band and the states below this level would be filled and unavailable for optical transitions from the valence band. As a consequence, the observed optical bandgap can in fact increase. This "Moss-Burstein" effect<sup>46</sup> can compensate or even dominate the aforementioned renormalization effect as has been shown in silicon- and germanium-doped wurtzite GaN.<sup>47</sup> To investigate if the dip in the bandgap observed in this work could be caused by renormalization, we simulated band bending and electron accumulation at the interface with a one-dimensional (1D) Poisson solver, BandEng, from UCSB. 48 The analysis is especially straightforward and in line with the common anion rule 49 because our DFT calculations show that the VB has no offset across the interface, and the entire offset of 0.24 eV is located in the CB. With that, we have set up our interface system in BandEng and studied different doping scenarios. Because commercial  $\beta$ -Ga<sub>2</sub>O<sub>3</sub> substrates are typically n-type with electron concentrations of, for example, 10<sup>17</sup> cm -350 and our DFT calculations show that the observed interstitials should be donors (Figure S7b), n-n junctions are the most relevant case for the example of doping levels of 10<sup>19</sup> cm<sup>-3</sup> as shown in Figure S6. Even at this relatively moderate doping level as compared to 10<sup>21</sup> cm<sup>-3</sup> required to renormalize the bandgap by 0.1 eV, the Moss-Borstein effect already adds at least that much to the observed bandgap, making this an unlikely explanation.

Alternatively, the bandgap shrinkage could also be due to excitonic absorption that happens in the vicinity of the interface as has been observed for n-n GaAs-(AlGa)As junctions. The calculated exciton binding energy in  $\beta$ -Ga<sub>2</sub>O<sub>3</sub> is 0.27 eV, <sup>52</sup> which, considering the broadening from

delocalization in experiment estimated to be  $\sim 15$  nm, could indeed result in the broad dip observed (compared to Figure 3). Although no observations of excitons have been reported in  $\beta$ -Ga<sub>2</sub>O<sub>3</sub> using EELS, the detection of multiple excitons in other nanostructures are reported using monochromated EELS with the energy resolution on the order of 20 meV or below. S3-S5 From our current data, it is not possible to unambiguously confirm the presence of the excitons with our current experimental conditions and energy resolution (125 meV). The lack of sufficient spectral resolution in particular can lead to peak broadening and can further convolute the bandgap and the exciton peak, making it impossible to separate out the two phenomena. Further studies with higher spectral resolution and potentially at low temperatures are necessary to uncover excitonic fingerprints in the sample.

Finally, the bandgap can also decrease due to the presence of defects, which is the prevalent hypothesis in the literature. For example, in ref 44, it is found that defects in thin undoped  $\beta$ -Ga<sub>2</sub>O<sub>3</sub> films lower the observed optical bandgap from 4.85 to 4.57 eV. Using deep-level transient spectroscopy, this study shows several deep level states, ~0.5-0.7 eV, below the conduction band. By analogy to other oxides of the observed life times in positron annihilation studies, the defects are interpreted as cation vacancies, although no more direct proof is given. Ga-vacancies, or divacancy Ga-interstitial complexes, have been observed more directly by electron microscopy in ref 56 with deep levels in the gap, making this a viable hypothesis. The observed interstitials at the interface have in theory deep levels (Figure S7b) or could be paired with vacancies that do not show in direct observation. However, they are located right at the interface (Figure 1), whereas the minimum of the dip is ~14 nm away from it (Figure S5), making this implausible. Still, the assumption that we have a high concentration of vacancies that exponentially decline into the  $\beta$ -Ga<sub>2</sub>O<sub>3</sub> substrate could lead to the observed dip in the bandgap. To demonstrate that, we assume that the bandgap in the substrate next to the interface has the value of 4.57 eV measured in ref 44 whereas the rate of increase is unknown. The electron probe typically has a delocalization effect of a few nanometers in VEELS. To simulate the delocalization of the electron beam, we convolute the exponential change in the bandgap with a Lorentzian function which results in 15 nm broadening. We then adjust the exponential decay constant to see if the experimental VEELS-measured bandgap across the interface can be reproduced. Figure 3 shows an exponential decay length of 7 nm (red dashed line), convoluted with 15 nm Lorentzian broadening (red solid line). This results in a curve that matches the experimental curve with an apparent dip on the  $\beta$ -Ga<sub>2</sub>O<sub>3</sub> side whose shape is to a large degree due to the deconvolution broadening, which has been shown to be between a few and tens of nm.

Summarizing our findings, our results give strong indication that there is no combination of doping between the  $\beta$ -(Al<sub>0.2</sub>Ga<sub>0.8</sub>)<sub>2</sub>O<sub>3</sub> film and substrate that would result in a dip on the  $\beta$ -Ga<sub>2</sub>O<sub>3</sub> side of the interface from electronic and bandbending effects, leaving the origin of the dip to an effect that decreases the bandgap at, or right below the interface. However, the presence of defects such as cation vacancies in  $\beta$ -Ga<sub>2</sub>O<sub>3</sub> or possible excitonic absorption could be plausibly responsible for the bandgap shrinkage. The sensible explanations require a strong broadening effect at the interface, which would be consistent with the delocalization broadening of the electron probe.

## CONCLUSIONS

In conclusion, spatially resolved bandgap variations across the  $\beta$ - $(Al_{1-x}Ga_x)_2O_3/\beta$ - $Ga_2O_3$  interface have been investigated by STEM-VEELS. The bandgap mean values for the  $\beta$ - $(Al_{0.2}Ga_{0.8})_2O_3$  thin film and for the  $\beta$ -Ga<sub>2</sub>O<sub>3</sub> substrate were  $E_{\rm g}$  = 5.04  $\pm$  0.1 eV and  $E_{\rm g}$  = 4.79  $\pm$  0.1 eV, respectively. A local dip of  $\sim$ 0.1 eV in the bandgap energy is observed near the  $\beta$ - $(Al_{0.2}Ga_{0.8})_2O_3/\beta$ -Ga<sub>2</sub>O<sub>3</sub> interface at the top of the  $\beta$ -Ga<sub>2</sub>O<sub>3</sub> substrate. Plausibility arguments have been given that this dip could be due to the presence of vacancies on the  $\beta$ -Ga<sub>2</sub>O<sub>3</sub> side of the interface or from excitonic absorptions though a final confirmation requires additional work. The shape and position of the dip seem to be considerably affected by the electron probe delocalization broadening. This work brings new insights into the impact of crystal defects on the electronic properties of  $\beta$ -(Al<sub>1-x</sub>Ga<sub>x</sub>)<sub>2</sub>O<sub>3</sub> films and clearly suggests that defects need to be well controlled in  $\beta$ -(Al<sub>1-x</sub>Ga<sub>x</sub>)<sub>2</sub>O<sub>3</sub>-based device fabrication.

## MATERIALS AND METHODS

**TEM Sample Preparation.** The TEM lamella was prepared using a Ga ion beam of a Thermo Scientific Scios DualBeam focused ion beam system. First, the bulk sample was taped to a focused ion beam stub with a carbon tape and a thin, 15 nm layer of carbon was deposited for better electrical conductivity. The sample was then polished down to an approximate thickness of 20 nm, followed by 2 h of polishing at 1 kV and 8 pA.

Material Characterization. Low-loss EELS measurements were performed using a double Cs corrected FEI Titan G2 60-300 transmission electron microscope equipped with a monochromator. With this equipment, an energy resolution of about 0.125 eV at fwhm of the ZLP is achieved. An accelerating voltage of 80 keV was used with convergence and collection semiangles of 11 and 9.2 mrad, respectively. EELS line scans were acquired using an energy dispersion of 0.025 eV/ch with a maximum pixel time of 0.5 s to avoid detector saturation. The distance between two consecutive VEELS spectra was 1.2 nm. With a duration of a line scan set around 8 and 15 min, the typical bandgap of  $\beta$ -Ga<sub>2</sub>O<sub>3</sub> is around 4.8 eV, close to the ZLP tail, thus, the latter has to be deconvoluted to remove plural scattering from the low-loss spectrum. The deconvolution was systematically done on each spectrum of the line scan acquisition by fitting a power law curve in a region of interest (typically between 2 and 4 eV) in which the background is easily discernible. Highresolution HAADF-STEM images were obtained using an acceleration voltage of 300 kV with a HAADF detector that collects scattering angles in the 42-244 mrads range.

**Image Simulations.** HAADF–STEM image simulations were performed using MacTempas software within the multi-slice method. The simulated TEM parameters were the following: HT = 300 kV, Cs =  $-1~\mu$ m, and C<sub>5</sub> = 2 mm. Each simulation was performed in a 30 nm thick  $\beta$ -(Al<sub>0.2</sub>Ga<sub>0.8</sub>)<sub>2</sub>O<sub>3</sub> supercell generated by DFT containing approximately 80 Ga atoms per atomic column.

**DFT Calculations.** DFT calculations for bulk are performed on a 1  $\times$  5  $\times$  2 supercell of  $\beta$ -(Al<sub>0.2</sub>Ga<sub>0.8</sub>)<sub>2</sub>O<sub>3</sub> containing 200 atoms. The supercell was generated as a special quasi-random structure<sup>58</sup> using the mcsqs code of the Alloy Theoretic Automated Toolkit.<sup>59</sup> DFT calculations have been carried out with the Vienna ab initio simulation package,<sup>60</sup> using Perdew–Burke–Ernzerhof functionals implemented in the AM05<sup>61</sup> parameterization of the generalized gradient approximation.<sup>62</sup> The relaxed configuration was obtained using a 3  $\times$  3  $\times$  3 k-point grid and a plane-wave energy cutoff of 400 eV. A pseudomorphic film on top of  $\beta$ -Ga<sub>2</sub>O<sub>3</sub> was assumed for the  $\beta$ -(Al<sub>0.2</sub>Ga<sub>0.8</sub>)<sub>2</sub>O<sub>3</sub>/ $\beta$ -Ga<sub>2</sub>O<sub>3</sub> interface and all atomic positions and the out-of-plane lattice constant were relaxed, whereas the in-plane lattice constants were kept fixed to those of  $\beta$ -Ga<sub>2</sub>O<sub>3</sub>. Band structure calculations were performed by meta-generalized gradient approximation calculations with the SCAN functional.<sup>63</sup>

#### ASSOCIATED CONTENT

# **Solution** Supporting Information

The Supporting Information is available free of charge at https://pubs.acs.org/doi/10.1021/acsaelm.1c00824.

EDS mapping of Al, Ga, and O elements across the  $\beta$ - $(Al_{0.2}Ga_{0.8})_2O_3/\beta$ - $Ga_2O_3$  interface;  $\beta$ - $(Al_{0.2}Ga_{0.8})_2O_3$  crystal structure model within one Al interstitial and its resulting HAADF–STEM simulation; lattice parameter variation for  $\beta$ - $Ga_2O_3$ ,  $Al_2O_3$ , and  $\beta$ - $(Ga_{0.8}Al_{0.2})_2O_3$ ; geometric phase analysis across the  $\beta$ - $(Al_{0.2}Ga_{0.8})_2O_3/\beta$ - $Ga_2O_3$  interface as shown in the HAADF–STEM image; bandgap variation superimposed with HAADF contrast variation along the line scan; BandEng 1D Poisson solver results for an  $(Al_{0.2}Ga_{0.8})_2O_3/Ga_2O_3$  interface with electron concentrations of  $10^{19}$  cm<sup>-3</sup>; DFT results for band structures of a  $1 \times 5 \times 2$   $\beta$ - $(Al_{0.2}Ga_{0.8})_2O_3$  supercell; and DFT results for bandgap renormalization in  $\beta$ - $Ga_2O_3$  as a function of the doping level (PDF)

# AUTHOR INFORMATION

# **Corresponding Author**

Nasim Alem — Department of Materials Science and Engineering, Materials Research Institute, The Pennsylvania State University, University Park 16802, United States;
ocid.org/0000-0003-0009-349X; Email: nua10@psu.edu

#### **Authors**

Adrian Chmielewski — Department of Materials Science and Engineering, Materials Research Institute, The Pennsylvania State University, University Park 16802, United States;
ocid.org/0000-0003-2373-5061

Ziling Deng – Department of Materials Science and Engineering, The Ohio State University, Columbus, Ohio 43210, United States

Parivash Moradifar – Department of Materials Science and Engineering, Materials Research Institute, The Pennsylvania State University, University Park 16802, United States

Leixin Miao – Department of Materials Science and Engineering, Materials Research Institute, The Pennsylvania State University, University Park 16802, United States

Yuewei Zhang — Materials Department, University of California Santa Barbara, Santa Barbara, California 93106, United States

Akhil Mauze – Materials Department, University of California Santa Barbara, Santa Barbara, California 93106, United States

Kleyser A. Lopez – Department of Materials Science and Engineering, Materials Research Institute, The Pennsylvania State University, University Park 16802, United States

Wolfgang Windl – Department of Materials Science and Engineering, The Ohio State University, Columbus, Ohio 43210, United States

Complete contact information is available at: https://pubs.acs.org/10.1021/acsaelm.1c00824

## Notes

The authors declare no competing financial interest.

## ACKNOWLEDGMENTS

N.A. would like to acknowledge Prof. James Speck for initial discussions regarding this manuscript. The authors thank Prof.

Roberto Myers for fruitful discussions concerning the interpretation of the measured results. The work at PSU was supported in part by the Air Force Office of Scientific Research (AFOSR) program FA9550-18-1-027. The work at OSU was supported by AFOSR program FA9550-18-1-0335. The work at UCSB was supported in part by the AFOSR program FA9550-18-1-0479 (GAME MURI, Dr. Ali Sayir, Program Manager). Any opinions, findings and conclusions or recommendations in this material are those of the authors and do not necessarily reflect the views of the United States Air Force. P.M.'s and K.A.L.'s work was supported by the National Science Foundation through the Penn State MRSEC, the Center for Nanoscale Science, under grant number DMR-140620. L.M.'s work was supported by the Penn State Center for Nanoscale Sciences, an NSF MRSEC under the grant number DMR-2011839 (2020-2026).

### REFERENCES

- (1) Higashiwaki, M.; Sasaki, K.; Murakami, H.; Kumagai, Y.; Koukitu, A.; Kuramata, A.; Masui, T.; Yamakoshi, S. Recent Progress In Ga2o3power Devices. *Semicond. Sci. Technol.* **2016**, *31*, 034001.
- (2) Pearton, S. J.; Yang, J.; Cary, P. H.; Ren, F.; Kim, J.; Tadjer, M. J.; Mastro, M. A. A Review Of Ga2o3materials, Processing, And Devices. *Appl. Phys. Rev.* **2018**, *5*, 011301.
- (3) Weng, W. Y.; Hsueh, T. J.; Chang, S. J.; Hung, S. C.; Huang, G. J.; Hsueh, H. T.; Huang, Z. D.; Chiu, C. J. An  $\{(\{\Rm Al}_{\Rm X}_{\Rm Ga}_{1-\{\Rm X}\})\}_{2}_{\Rm O}_{3}$  Metal-Semi-conductor-Metal VUV Photodetector. *IEEE Sensor. J.* **2011**, *11*, 1795–1799.
- (4) Zhang, D.; Lin, W.; Liu, S.; Zhu, Y.; Lin, R.; Zheng, W.; Huang, F. Ultra-Robust Deep-UV Photovoltaic Detector Based On Graphene/(Alga)2O3/Gan With High-Performance In Temperature Fluctuations. ACS Appl. Mater. Interfaces 2019, 11, 48071–48078.
- (5) Shi, J.; Liang, H.; Xia, X.; Long, Z.; Zhang, H.; Liu, Y.; Dong, X.; Jia, Z. Preparation Of High Al Content (Alxga1–X)2O3 Films By Low-Pressure Reactive Vapor Deposition On Sapphire Substrates. ECS J. Solid State Sci. Technol. 2020, 9, 045016.
- (6) Ratnaparkhe, A.; Lambrecht, W. R. L. Quasiparticle Self-Consistent GW Study Of (Ga 1- X Al X ) 2 O 3 Alloys In Monoclinic And Corundum Structures. *Phys. Status Solidi B* **2019**, 257, 1900317.
- (7) Lyle, L. A. M.; Okur, S.; Chava, V. S. N.; Kelley, M. L.; Davis, R. F.; Tompa, G. S.; Chandrashekhar, M. V. S.; Greytak, A. B.; Porter, L. M. Characterization Of Epitaxial B-(Al,Ga,In)2O3-Based Films And Applications As UV Photodetectors. *J. Electron. Mater.* **2020**, 49, 3490–3498.
- (8) Liao, C.-H.; Li, K.-H.; Torres-Castanedo, C. G.; Zhang, G.; Li, X. Wide Range Tunable Bandgap And Composition B-Phase (Alga)2O3 Thin Film By Thermal Annealing. *Appl. Phys. Lett.* **2021**, *118*, 032103.
- (9) Li, J.; Chen, X.; Ma, T.; Cui, X.; Ren, F.-F.; Gu, S.; Zhang, R.; Zheng, Y.; Ringer, S. P.; Fu, L.; et al. Identification And Modulation Of Electronic Band Structures Of Single-Phase B-(Alxga1-X)2O3 Alloys Grown By Laser Molecular Beam Epitaxy. *Appl. Phys. Lett.* **2018**, *113*, 041901.
- (10) Wang, T.; Li, W.; Ni, C.; Janotti, A. Band Gap And Band Offset Of Ga2o3 And (Alxga1-X)2O3 Alloys. *Phys. Rev. Appl.* **2018**, *10*, 011003.
- (11) Peelaers, H.; Varley, J. B.; Speck, J. S.; Van de Walle, C. G. Structural And Electronic Properties Of Ga2o3-Al2o3 Alloys. *Appl. Phys. Lett.* **2018**, *112*, 242101.
- (12) Feng, Q.; Li, X.; Han, G.; Huang, L.; Li, F.; Tang, W.; Zhang, J.; Hao, Y. (Alga)\_2O\_3 Solar-Blind Photodetectors On Sapphire With Wider Bandgap And Improved Responsivity. *Opt. Mater. Express* **2017**, *7*, 1240.
- (13) Schmidt-Grund, R.; Kranert, C.; von Wenckstern, H.; Zviagin, V.; Lorenz, M.; Grundmann, M. Dielectric Function In The Spectral

- Range (0.5–8.5)Ev Of An (Alx Ga1–X)2O3 Thin Film With Continuous Composition Spread. *J. Appl. Phys.* **2015**, *117*, 165307.
- (14) Onuma, T.; Saito, S.; Sasaki, K.; Masui, T.; Yamaguchi, T.; Honda, T.; Higashiwaki, M. Valence Band Ordering In B-Ga2o3studied By Polarized Transmittance And Reflectance Spectroscopy. *Jpn. J. Appl. Phys.* **2015**, *54*, 112601.
- (15) Zhang, F.; Saito, K.; Tanaka, T.; Nishio, M.; Arita, M.; Guo, Q. Wide Bandgap Engineering Of (Alga)2O3 Films. *Appl. Phys. Lett.* **2014**, *105*, 162107.
- (16) Krueger, B. W.; Dandeneau, C. S.; Nelson, E. M.; Dunham, S. T.; Ohuchi, F. S.; Olmstead, M. A. Variation Of Band Gap And Lattice Parameters Of B—(Al X Ga 1— X ) 2 O 3 Powder Produced By Solution Combustion Synthesis. *J. Am. Ceram. Soc.* **2016**, 99, 2467—2473.
- (17) French, R. H.; Müllejans, H. Quantitative Analysis Of Valence Electron Energy-Loss Spectra Of Aluminium Nitride. *J. Microsc.* **1998**, 191, 286–296.
- (18) Erni, R.; Browning, N. D. Valence Electron Energy-Loss Spectroscopy In Monochromated Scanning Transmission Electron Microscopy. *Ultramicroscopy* **2005**, *104*, 176–192.
- (19) Egerton, R. F. Physics of Electron Scattering. *Electron. Energy Loss Spectrosc. Electron Microsc.* **2011**, 111–229.
- (20) Pines, D. Elementary Excitations in Solids Lectures on Protons Electrons, and Plasmons; CRC Press, 1999.
- (21) Stöger-Pollach, M.; Laister, A.; Schattschneider, P. Treating Retardation Effects In Valence EELS Spectra For Kramers-Kronig Analysis. *Ultramicroscopy* **2008**, *108*, 439–444.
- (22) Egerton, R. F. Electron Energy-Loss Spectroscopy in the Electron Microscope; Springer Science & Business Media, 2011; pp 1–28.
- (23) Bangert, U.; Harvey, A. J.; Keyse, R. Assessment Of Electron Energy-Loss Spectroscopy Below 5 Ev In Semiconductor Materials In A VG STEM. *Ultramicroscopy* **1997**, *68*, 173–180.
- (24) Rafferty, B.; Brown, L. M. Direct And Indirect Transitions In The Region Of The Band Gap Using Electron-Energy-Loss Spectroscopy. *Phys. Rev. B: Condens. Matter Mater. Phys.* **1998**, *58*, 10326–10337.
- (25) Hachtel, J. A.; Lupini, A. R.; Idrobo, J. C. Exploring The Capabilities Of Monochromated Electron Energy Loss Spectroscopy In The Infrared Regime. *Sci. Rep.* **2018**, *8*, 1.
- (26) Kimoto, K.; Kothleitner, G.; Grogger, W.; Matsui, Y.; Hofer, F. Advantages Of A Monochromator For Bandgap Measurements Using Electron Energy-Loss Spectroscopy. *Micron* **2005**, *36*, 185–189.
- (27) Zhan, W.; Granerød, C. S.; Venkatachalapathy, V.; Johansen, K. M. H.; Jensen, I. J. T.; Kuznetsov, A. Y.; Prytz, Ø. Nanoscale Mapping Of Optical Band Gaps Using Monochromated Electron Energy Loss Spectroscopy. *Nanotechnology* **2017**, *28*, 105703.
- (28) Keller, D.; Buecheler, S.; Reinhard, P.; Pianezzi, F.; Pohl, D.; Surrey, A.; Rellinghaus, B.; Erni, R.; Tiwari, A. N. Local Band Gap Measurements By VEELS Of Thin Film Solar Cells. *Microsc. Microanal.* **2014**, *20*, 1246–1253.
- (29) Park, J.; Heo, S.; Chung, J.-G.; Kim, H.; Lee, H.; Kim, K.; Park, G.-S. Bandgap Measurement Of Thin Dielectric Films Using Monochromated STEM-EELS. *Ultramicroscopy* **2009**, *109*, 1183–1188
- (30) Virdi, K. S.; Kauffmann, Y.; Ziegler, C.; Ganter, P.; Blaha, P.; Lotsch, B. V.; Kaplan, W. D.; Scheu, C. Band Gap Extraction From Individual Two-Dimensional Perovskite Nanosheets Using Valence Electron Energy Loss Spectroscopy. *J. Phys. Chem. C* **2016**, 120, 11170–11179.
- (31) Park, J.; Yang, M. Determination Of Complex Dielectric Functions At Hfo2/Si Interface By Using STEM-VEELS. *Micron* **2009**, *40*, 365–369.
- (32) Cañas, J.; Piñero, J.; Lloret, F.; Gutierrez, M.; Pham, T.; Pernot, J.; Araujo, D. Determination Of Alumina Bandgap And Dielectric Functions Of Diamond MOS By STEM-VEELS. *Appl. Surf. Sci.* **2018**, 461, 93–97.
- (33) Brockt, G.; Lakner, H. Nanoscale EELS Analysis Of Dielectric Function And Bandgap Properties In Gan And Related Materials. *Micron* **2000**, *31*, 435–440.

- (34) Potapov, P. L.; Engelmann, H.-J.; Zschech, E.; Stöger-Pollach, M. Measuring The Dielectric Constant Of Materials From Valence EELS. *Micron* **2009**, *40*, 262–268.
- (35) Lyu, F.; Sun, Y.; Yang, Q.; Tang, B.; Li, M.; Li, Z.; Sun, M.; Gao, P.; Ye, L.-H.; Chen, Q. Thickness-Dependent Band Gap Of A-In2se3: From Electron Energy Loss Spectroscopy To Density Functional Theory Calculations. *Nanotechnology* **2020**, *31*, 315711.
- (36) Ranga, P.; Rishinaramangalam, A.; Varley, J.; Bhattacharyya, A.; Feezell, D.; Krishnamoorthy, S. Si-Doped B-(Al0.26Ga0.74)2O3 Thin Films And Heterostructures Grown By Metalorganic Vapor-Phase Epitaxy. *Appl. Phys. Express* **2019**, *12*, 111004.
- (37) Bhuiyan, A. F. M. A. U.; Feng, Z.; Johnson, J. M.; Chen, Z.; Huang, H.-L.; Hwang, J.; Zhao, H. MOCVD Epitaxy Of B-(Alxga1–X)2O3 Thin Films On (010) Ga2o3 Substrates And N-Type Doping. *Appl. Phys. Lett.* **2019**, *115*, 120602.
- (38) Bhuiyan, A. F. M. A. U.; Feng, Z.; Johnson, J. M.; Huang, H.-L.; Sarker, J.; Zhu, M.; Karim, M. R.; Mazumder, B.; Hwang, J.; Zhao, H. Phase Transformation In MOCVD Growth Of (Alxga1—X)2O3 Thin Films. *APL Mater.* **2020**, *8*, 031104.
- (39) Sarker, J.; Bhuiyan, A. F. M. A. U.; Feng, Z.; Zhao, H.; Mazumder, B. Direct Observation Of Site-Specific Dopant Substitution In Si Doped (Al X Ga1— X )2O3 Via Atom Probe Tomography. *J. Phys. D: Appl. Phys.* **2021**, *54*, 184001.
- (40) Schmidt-Grund, R.; Kranert, C.; von Wenckstern, H.; Zviagin, V.; Lorenz, M.; Grundmann, M. Dielectric Function In The Spectral Range (0.5–8.5)Ev Of An (Alx Ga1–X)2O3 Thin Film With Continuous Composition Spread. *J. Appl. Phys.* **2015**, *117*, 165307.
- (41) Vogt, P.; Mauze, A.; Wu, F.; Bonef, B.; Speck, J. S. Metal-Oxide Catalyzed Epitaxy (MOCATAXY): The Example Of The O Plasma-Assisted Molecular Beam Epitaxy Of B-(Al X Ga1- X )2O3/B-Ga2o3 Heterostructures. *Appl. Phys. Express* **2018**, *11*, 115503.
- (42) Johnson, J. M.; Huang, H.-L.; Wang, M.; Mu, S.; Varley, J. B.; Uddin Bhuiyan, A. F. M. A.; Feng, Z.; Kalarickal, N. K.; Rajan, S.; Zhao, H.; et al. Atomic Scale Investigation Of Aluminum Incorporation, Defects, And Phase Stability In B-(Alxga1–X)2O3 Films. *APL Mater.* **2021**, *9*, 051103.
- (43) Jin, H.; Oh, S. K.; Kang, H. J. Electronic Structure Of Ultrathin Si Oxynitrides. *Surf. Interface Anal.* **2006**, *38*, 1564–1567.
- (44) Saadatkia, P.; Agarwal, S.; Hernandez, A.; Reed, E.; Brackenbury, I.; Codding, C.; Liedke, M.; Butterling, M.; Wagner, A.; Selim, F. Point And Extended Defects In Heteroepitaxial B–Ga2o3 Films. *Phys. Rev. Mater.* **2020**, *4*, 104602.
- (45) Berggren, K.-F.; Sernelius, B. E. Band-Gap Narrowing In Heavily Doped Many-Valley Semiconductors. *Phys. Rev. B: Condens. Matter Mater. Phys.* **1981**, 24, 1971–1986.
- (46) Burstein, E. Anomalous Optical Absorption Limit In Insb. *Phys. Rev.* **1954**, 93, 632–633.
- (47) Feneberg, M.; Osterburg, S.; Lange, K.; Lidig, C.; Garke, B.; Goldhahn, R.; Richter, E.; Netzel, C.; Neumann, M.; Esser, N.; et al. Band Gap Renormalization And Burstein-Moss Effect In Silicon- And Germanium-Doped Wurtzite Gan Up To1020 Cm—3. *Phys. Rev. B: Condens. Matter Mater. Phys.* **2014**, *90*, 075203.
- (48) Grundmann, M. http://my.ece.ucsb.edu/mgrundmann/bandeng/, 2007 (accessed Dec 10, 2021).
- (49) McCaldin, J. O.; McGill, T. C.; Mead, C. A. Correlation For III-V And II-VI Semiconductors Of The Au Schottky Barrier Energy With Anion Electronegativity. *Phys. Rev. Lett.* **1976**, *36*, 56–58.
- (50) Ma, N.; Tanen, N.; Verma, A.; Guo, Z.; Luo, T.; Xing, H.; Jena, D. Intrinsic Electron Mobility Limits In $\beta$ -Ga2o3. *Appl. Phys. Lett.* **2016**, *109*, 212101.
- (51) Balslev, I. Recombination Via Two-Dimensional Excitons In Gaas-(Alga)As Heterojunctions. *Semicond. Sci. Technol.* **1987**, 2, 437–441.
- (52) Sturm, C.; Schmidt-Grund, R.; Kranert, C.; Furthmüller, J.; Bechstedt, F.; Grundmann, M. Dipole Analysis Of The Dielectric Function Of Color Dispersive Materials: Application To Monoclinicga2o3. *Phys. Rev. B: Condens. Matter Mater. Phys.* **2016**, 94, 035148.

- (53) Gogoi, P. K.; Lin, Y.-C.; Senga, R.; Komsa, H.-P.; Wong, S. L.; Chi, D.; Krasheninnikov, A. V.; Li, L.-J.; Breese, M. B. H.; Pennycook, S. J.; et al. Layer Rotation-Angle-Dependent Excitonic Absorption In Van Der Waals Heterostructures Revealed By Electron Energy Loss Spectroscopy. *ACS Nano* **2019**, *13*, 9541–9550.
- (54) Nerl, H.; Winther, K.; Hage, F.; Thygesen, K.; Houben, L.; Backes, C.; Coleman, J.; Ramasse, Q.; Nicolosi, V. Probing The Local Nature Of Excitons And Plasmons In Few-Layer Mos2. *npj 2D Mater. Appl.* **2017**, *1*, 1.
- (55) Tizei, L. H. G.; Lin, Y.-C.; Lu, A.-Y.; Li, L.-J.; Suenaga, K. Electron Energy Loss Spectroscopy Of Excitons In Two-Dimensional-Semiconductors As A Function Of Temperature. *Appl. Phys. Lett.* **2016**, *108*, 163107.
- (56) Johnson, J.; Chen, Z.; Varley, J.; Jackson, C.; Farzana, E.; Zhang, Z.; Arehart, A.; Huang, H.; Genc, A.; Ringel, S.; et al. Unusual Formation Of Point-Defect Complexes In The Ultrawide-Band-Gap Semiconductor B—Ga2o3. *Phys. Rev. X* **2019**, *9*, 041027.
- (57) Egerton, R. F. Scattering Delocalization And Radiation Damage In STEM-EELS. *Ultramicroscopy* **2017**, *180*, 115–124.
- (58) Zunger, A.; Wei, S.-H.; Ferreira, L. G.; Bernard, J. E. Special Quasirandom Structures. *Phys. Rev. Lett.* **1990**, *65*, 353–356.
- (59) van de Walle, A.; Tiwary, P.; de Jong, M.; Olmsted, D. L.; Asta, M.; Dick, A.; Shin, D.; Wang, Y.; Chen, L.-Q.; Liu, Z.-K. Efficient Stochastic Generation Of Special Quasirandom Structures. *Calphad* **2013**, *42*, 13–18.
- (60) Kresse, G.; Furthmüller, J. Efficient Iterative Schemes Forab Initiototal-Energy Calculations Using A Plane-Wave Basis Set. *Phys. Rev. B: Condens. Matter Mater. Phys.* **1996**, *54*, 11169–11186.
- (61) Armiento, R.; Mattsson, A. Functional Designed To Include Surface Effects In Self-Consistent Density Functional Theory. *Phys. Rev. B: Condens. Matter Mater. Phys.* **2005**, 72, 085108.
- (62) Perdew, J. P.; Burke, K.; Ernzerhof, M. Generalized Gradient Approximation Made Simple. *Phys. Rev. Lett.* **1996**, *77*, 3865–3868.
- (63) Sun, J.; Ruzsinszky, A.; Perdew, J. Strongly Constrained And Appropriately Normed Semilocal Density Functional. *Phys. Rev. Lett.* **2015**, *115*, 036402.